Lattice dynamics and structural stability of ordered Fe_3Ni, Fe_3Pd and Fe_3Pt alloys using density functional theory

M. E. Gruner,[1,*] W. A. Adeagbo,[2] A. T. Zayak,[3,4] A. Hucht,[1] and P. Entel[1]
[1]*Faculty of Physics and Center for Nanointegration, CeNIDE, University of Duisburg-Essen, 47048 Duisburg, Germany*
[2]*Institute of Physics, Martin Luther University Halle-Wittenberg, 06120 Halle, Germany*
[3]*Department of Electrical Engineering and Computer Sciences, University of California, Berkeley, California 94720, USA*
[4]*Molecular Foundry, Lawrence Berkeley National Laboratory, Berkeley, California 94720, USA*
(Received 22 November 2009; revised manuscript received 25 January 2010; published 16 February 2010)

We investigate the binding surface along the Bain path and phonon dispersion relations for the cubic phase of the ferromagnetic binary alloys $Fe_3X(X=Ni,Pd,Pt)$ for $L1_2$ and $D0_{22}$ ordered phases from first principles by means of density functional theory. The phonon dispersion relations exhibit a softening of the transverse acoustic mode at the M point in the $L1_2$ phase in accordance with experiments for ordered Fe_3Pt. This instability can be associated with a rotational movement of the Fe atoms around the Ni-group element in the neighboring layers and is accompanied by an extensive reconstruction of the Fermi surface. In addition, we find an incomplete softening in [111] direction which is strongest for Fe_3Ni. We conclude that besides the valence electron density also the specific Fe-content and the masses of the alloying partners should be considered as parameters for the design of Fe-based functional magnetic materials.

DOI: 10.1103/PhysRevB.81.064109 PACS number(s): 63.20.kd, 75.50.Bb, 71.18.+y, 81.30.Kf

I. INTRODUCTION

Ferrous alloys are well known for a wide variety of anomalous structural and magnetic properties. Around 1185 K, bulk iron undergoes a structural transition from a face centered cubic (fcc) high-temperature phase to a low-temperature body centered cubic (bcc) phase, which is ferromagnetic with a Curie temperature of 1043 K. The structural transition temperature is systematically lowered by alloying elements from the right side of Fe in the periodic table, which effectively lowers the valence electron concentration e/a. The transition is displacive and diffusionless between a high-temperature high-symmetry austenitic phase and a low-temperature martensitic phase, in which the symmetry is usually lowered, e.g., by tetragonal distortions. In ferromagnetic Fe-alloys with e/a between 8.7 and 8.5, the martensitic transition disappears and fcc austenite becomes the stable ground-state structure. Iron alloys with Ni-group elements at this valence electron concentration are at the center of scientific interest for a long time, as they show, in addition to the martensitic instability, a multitude of magnetostructural anomalies that are of technological importance. The probably most prominent is the so-called Invar effect, describing the over-compensation of thermal expansion in a wide temperature range, which has been intensively studied for more than one century.[1–3] The best known representative is $Fe_{65}Ni_{35}$, but similar behavior is also observed in $Fe_{70}Pd_{30}$ and $Fe_{75}Pt_{25}$. Although most explanations proposed so far rely on magnetovolume coupling, the vicinity to the martensitic transformation has been well noticed and discussed. The relevant literature on this topic is too numerous to be summarized at this point—for an introduction and further references, see, e.g., Refs. 4–6.

During the past three decades, the so-called magnetic shape memory (MSM) effect, which is again present in the alloys with all three Ni-group elements, was brought to the attention of the scientific community. The MSM behavior allows very large magnetic-field-induced strains of up to three percent to be achieved by externally applying moderate magnetic fields in the (sub-)Tesla range.[7–11] The effect is not as pronounced as for the Ni-based Heusler alloys such as Ni_2MnGa,[12–14] but its origin is believed to be related. One common key ingredient is the appearance of intermediate or modulated martensites—fivefold and tenfold modulated pseudotetragonal or orthohombic in the case of Ni-Mn-Ga (Refs. 15–17) and (slightly distorted) face centered tetragonal (fct) in the case of Fe-Pt and Fe-Pd—between the high symmetry austenite and the low-temperature martensite, which is body centered tetragonal in the case of the ferrous alloys.[18–20]

For the above mentioned alloys, the relevant electron concentration range is achieved at compositions which may allow the formation of ordered stoichiometric compounds. However, Fe_3Pt is the only alloy where the ordered phase is reproducibly realized in experiment. Nevertheless, measurements are predominately made for slightly off-stoichiometric ordered $Fe_{72}Pt_{28}$ which does not transform martensitically, even if order is not fully complete. Therefore, most data are available only for disordered or partially ordered alloys. Despite this fact, we will restrict our study to stoichiometric, ordered compounds. These are much easier to handle from the technical point of view and allow deeper insight into electronic and vibrational properties with respect to their physical origin, because their simulation cells are sufficiently small while side-effects as statistical broadening can be largely avoided.

Another important feature of these alloys is the marked softening of the transversal acoustic phonons in [110] direction, which has subsequently been related to any of the three above mentioned anomalies in the past.[21–29] Our central aim is thus to investigate the influence of electron-phonon coupling in Fe_3Ni, Fe_3Pd, and Fe_3Pt as one of the important mechanisms for structural transformations of Fe-based binary alloys. This complements the experimental information

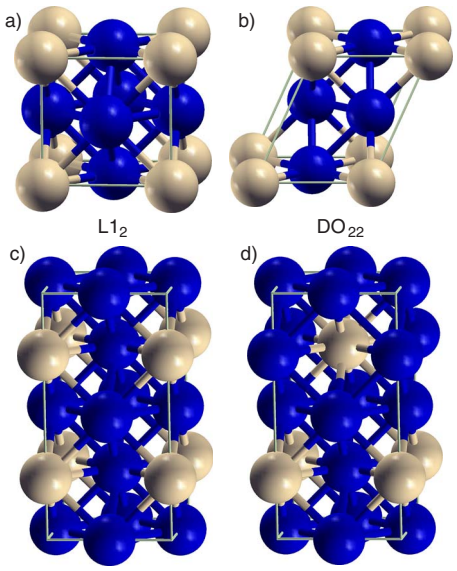

FIG. 1. (Color online) Primitive cells of fcc $L1_2$ (a) and $D0_{22}$ (b) ordered alloys of A_3B stoichiometry as used in our calculations. The lower two images show both structures represented in the same supercell which consists of two primitive cells stacked along the c axis in the case of $L2_1$ (c). Exchanging the A and B components, marked by dark (blue) and bright (orange) spheres in one of the a-b-planes yields the $D0_{22}$ ordering (d). Note, that the symmetry of the $D0_{22}$ structure is tetragonal. After reduction of the c/a ratio by a factor of $\sqrt{1/2}$, the cell transforms to the bcc-type $D0_3$ structure with cubic symmetry.

by providing a link between electronic properties and structural distortions, which will help to clarify the microscopic origin of these instabilities. We accomplished this aim by comparing features of the phonon dispersion with the electronic structure of these alloys. A similar approach has been used in the past to explore the nature of electron-phonon coupling in conventional and magnetic shape memory alloys.[30–34]

During our preoccupation with this topic, we noticed that investigations providing a structural and dynamical view of the field on the basis of first-principles calculations are sparse and performed with varying methodology, hindering a comparison of all three isoelectronic alloys on equal footing. We therefore decided to provide first a systematic survey of structural properties and lattice dynamics of ordered Fe-rich alloys with elements of the Ni group, thereby filling the above mentioned gap in existing literature. The experimentally observed order in Fe_3Pt is of $L1_2$ type, see Fig. 1. In our calculations, we will alternatively consider $D0_{22}$ order. For lattices with bcc coordination $D0_{22}$ becomes equivalent with $D0_3$ order, which is related to the $L2_1$ structure of ternary Heusler alloys.

Fe-rich Fe-Pd and Fe-Pt alloys close to the stoichiometric composition are reported to be collinear ferromagnets at low temperatures; we will therefore solely concentrate on the collinear ferromagnetic case. Excited noncollinear, ferri- and antiferromagnetic spin structures, which have been discussed with respect to the Invar effect,[35–37] would certainly be beneficial for a thorough understanding of the interdependence of lattice dynamics and finite temperature anomalies as MSM and Invar effect. These, however, are beyond the scope of the current work and are thus left open for future investigation.

II. NUMERICAL DETAILS

Our investigation of the structural and dynamic properties has been performed within the framework of density functional theory (DFT).[38] The majority of our results has been obtained using the Vienna *ab initio* Simulation package (VASP).[39,40] This code concentrates—as pseudopotential methods generally do—for efficiency reasons on the valence electrons for the description of the electronic structure. The VASP code provides, nevertheless, an excellent compromise between speed and accuracy as the interaction with core electrons is taken into account within the projector augmented wave (PAW) approach.[41] This yields results close to what is usually expected from other all electron methods. As we are dealing with Fe-rich compositions, the use of the generalized gradient approximation (GGA) is mandatory to obtain a correct description of the structural ground-state properties. For structural energies within small (four atom) cells corresponding to Figs. 1(a) and 1(b) we use a k-mesh containing at least 16384 k-points$\times$atoms in the full Brillouin zone. For the calculation of the density of states (DOS) the k-point density was increased to values of 131072 k-points$\times$atoms and 340736 k-points$\times$atoms for obtaining the Fermi surface in the four atom cell. The Brillouin zone integration was carried out using the tetrahedron method with Blöchl corrections.[42] Electronic self-consistency was assumed below a threshold difference of 1 μeV between two iteration. The VASP code is supplied with an extensive, well tested potential library which contains more than one pregenerated pseudopotential per element. These differ by number of electrons explicitly treated as valence or semicore states or are designed for different exchange-correlation functionals. In our case, the GGA formulations of Perdew and Wang (PW91) in connection with the spin-interpolation formula of Vosko, Wilk and Nusair as well as Perdew Burke and Ernzerhof (PBE) have been used.[43–46] The required cutoff of the plane wave basis depends on the exchange-correlation potential and was chosen as E_{cut}=335 eV (or larger) for PW91 and PBE together with the minimal basis explicitly describing the $3d^74s^1$ for Fe and $4d^95s^1$ for Pd (and correspondingly for Ni and Pt). In calculations explicitly considering the semicore p-electrons, E_{cut} was set to 367 eV for PBE and 438 eV for the PW91 pseudopotentials. A scalar relativistic formulation of the Hamiltonian was used throughout.[47]

A. Comparison between VASP and WIEN2K

Although the above mentioned technical differences with respect to the choice of the exchange-correlation functional and the basis size usually do not lead to qualitative changes of the results, we must be particularly careful in our case, because energy landscapes in the vicinity of a structural transformation can be essentially flat. This requires a higher accuracy, i.e., a better energy resolution. Therefore, we de-

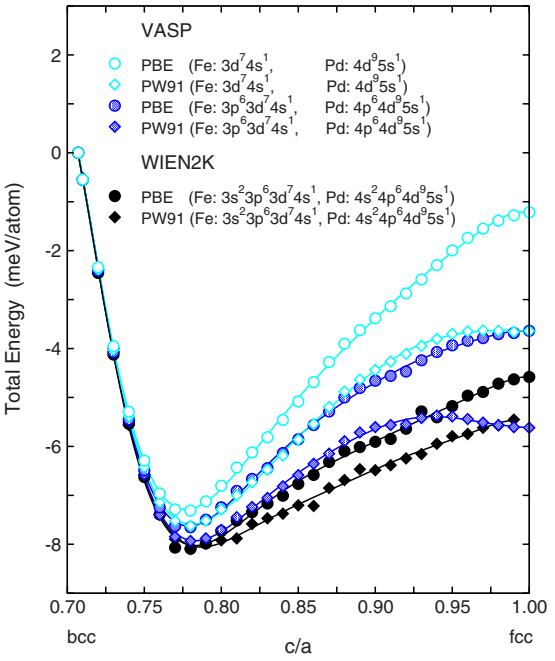

FIG. 2. (Color online) The energy profile along the Bain path for $L1_2Fe_3Pd$ obtained with VASP and WIEN2K for PBE and PW91 exchange-correlation potentials. The calculations were carried out at a fixed atomic volume of 13.08 Å^3, corresponding to an fcc lattice constant of $a=3.74$ Å. For better comparison, all results are given relative to the energy of the bcc state ($c/a=\sqrt{1/2}$). The labeling fcc and bcc refers to coordination of the atoms regardless of the species. With the VASP code, pseudopotentials with different numbers of semicore electrons were tested; the reference calculations (WIEN2K) account for Fe 3*s* and Pd 4*s* as semicore electrons. Most curves coincide along the full Bain path within 2 meV/atom.

cided to perform in a first step a thorough comparison of the available potentials. As a benchmark, we evaluated the energy as a function of the tetragonal distortion c/a along the Bain path[48] for $L1_2$ ordered Fe_3Pd, describing a structural deformation from a face centered cubic (fcc) lattice at $c/a=1$ to a body centered cubic (bcc) lattice at $c/a=\sqrt{1/2}$, as shown in Fig. 2. The results were compared to high precision calculations using the full potential linearized augmented plane wave method (FLAPW) as implemented within WIEN2K code,[49] which is widely counted among the most accurate DFT codes for solid state problems. Here, the calculations included 3*s* and 3*p* of iron and 4*s* and 4*p* of palladium as semicore. The energetic cutoff was chosen as $R_{\mathrm{MT}}\times K_{\max}=9.0$. Muffin-tin radii of 2.24 a.u. were used for all atoms and angular momenta were taken into account up to $l_{\max}=10$. The *k*-mesh comprised again 32000 *k*-points × atoms in the irreducible Brillouin zone.

The obtained energy variation along the Bain path is with ≈8 meV/atom very small. However, except for the PBE potentials without semicore *p* electrons, all curves coincide within an energy interval of 2…3 meV/atom (23…35 K on a temperature scale), which can be taken as a measure for the methodological resolution in calculating structural energy differences along the Bain path. While the PBE potentials seem to systematically overestimate the energy variation (slightly), the agreement between both PW91 potentials (large and small basis) and the full potential curves is very good. This finding agrees well with a recent comparison of experimental and theoretical structural data for equiatomic FePt alloys.[50] Our benchmark demonstrates that the accuracy of the PW91 pseudopotentials with the small basis (Fe 3*p* and Pd 4*p* as core electrons) is sufficient, which is especially helpful for expensive calculations of large systems.

B. Calculation of dynamical properties

Two standard techniques are currently applied for the investigation of lattice dynamics of crystals from first principles: the linear response method and the so-called direct method.[51–53] In the linear response method the dynamical matrix is obtained from the modification of the electron density, via the inverse of dielectric matrix describing the response of the valence electron density to a periodic lattice perturbation. The dielectric matrix is then calculated from the eigenfunctions and energy levels of the unperturbed system.[54] Only linear effects, such as harmonic phonons, are accessible to this technique. The method has been applied with success to many alloys related to our present study.[31,55]

On the other hand, the direct method is a frozen-phonon type of calculation based on a supercell which allows explicit account of any distortion of the atomic positions. The phonon frequencies are calculated from Hellmann-Feynman forces generated by the small atomic displacements, one at a time. Hence using the information of the crystal symmetry space group, the force constants are derived, the dynamical matrix is built and diagonalized, and its eigenvalues arranged into phonon dispersion relations. In this way, phonon frequencies at selected high-symmetry points of the Brillouin zone can be calculated.[56] The direct approach in conjunction with the *ab initio* method has previously been used intensively by the authors to investigate phonon dispersion relations in magnetic shape memory Heusler compounds.[32,57–59]

The results presented within this work are relying on the direct approach together with the VASP code for the calculation of the respective forces; the displacements being necessary to describe the phonon dispersions were generated by the PHON code written by Dario Alfè.[60,61] This code was also used later on to generate the dynamical matrix and the resulting phonon dispersion relations. We used a supercell of $5\times5\times5$ primitive cells, containing 500 atoms in total. For sufficient accuracy of the forces a *k* mesh of $4\times4\times4$ points in the full Brillouin zone was employed in connection with the Methfessel-Paxton finite temperature integration scheme (smearing parameter $\sigma=0.1$ eV). First-principles calculations of this size are computationally very demanding and can, so far, only be performed on world leading supercomputer installations. The forces were calculated for three independent displacements of 0.02 Å in size each. From these calculations the phonon dispersions along the lines connecting the main symmetry points and the vibrational density of states (VDOS) were calculated. For the latter, a mesh of $61\times61\times61$ points in reciprocal *q* space was used and additional Gaussian broadening with a smearing parameter of $\sigma=0.1$ THz was applied.

We also carried out comparative calculations for $D0_3Fe_3Ni$ and $L1_2Fe_3Pt$ using the linear response method as

implemented in the PWSCF package.[62] To describe the interaction between ionic cores and valence electrons, we used for Fe_3Ni ultrasoft pseudopotentials[63] generated using the exchange-correlation functional of Perdew, Burke, and Ernzerhof (PBE). The pseudopotentials for Fe_3Pt were generated for the exchange correlation of Perdew-Zunger within local density approximation (LDA).[64] The technical parameters used here, were a kinetic energy cutoff of 50 Ry, an energy cutoff for the augmentation charges of 600 Ry and $12\times12\times12$ k points in the full Brillouin zone (Monkhorst-Pack). For the phonon dispersions, a mesh of $4\times4\times4$ q points in the reciprocal space was used for the fcc basis, yielding eight sets with finite weight while for the simple cubic basis a $2\times2\times2$ q-points mesh was used yielding four sets of special q vectors with finite weight. Although the technical parameters are less tight, the obtained dispersions agree well on a qualitative level with the ones obtained within the direct approach (except for discrepancies which can be partially related to the use of LDA in the latter case as the typical underestimation of the lattice constant as well as an extension of the instability of the TA_1 branch to the Γ point, see also Ref. 65) and are therefore not explicitly presented in this paper.

III. COMPARISON OF STRUCTURAL PROPERTIES

There are a large number of reports of first principle investigations concerning Fe-rich alloys with elements of the platinum group available in literature. These cover magnetic and magnetoelastic properties,[66–72] electronic structure,[69,73–75] order and disorder.[76–78] Only few reports, however, are present describing the energetics of tetragonal distortions in ordered alloys. These exist, e.g., for Fe_3Pt using the linear muffin-tin orbital method within the atomic sphere approximation (LMTO-ASA) method and for Fe_3Ni using different approaches.[69,79–81] Again, particularly the FLAPW calculations of Ref. 81 agree very well with our results. A systematic *ab initio* comparison of all three alloys with respect to structural properties along the Bain path, describing the transformation from fcc-type to bcc-type structure, however, is still missing and therefore concisely presented in the subsequent section.

A. Binding surfaces along the Bain path

The total energy as a function of atomic volume and tetragonal distortion for all three isoelectronic alloys in $L1_2$ order is shown in Fig. 3. As is easily seen from the contour plots, the optimum c/a ratio varies from close to bcc ($c/a=0.74$) for Fe_3Ni over bct ($c/a=0.78$) for Fe_3Pd to fcc ($c/a=1$) for Fe_3Pt. This trend cannot simply be interpreted in terms of the atomic volume as, especially for Fe_3Pd and Fe_3Pt, the equilibrium volumes nearly coincide. This is in good agreement with experimental measurements (see the collection of Okamoto, Ref. 82, for an extensive overview). Especially the relation between lattice parameter and composition of Fe_3Pd exhibits a strong positive deviation from Vegards law. The overall variation in the energy landscape along the Bain path is exceptionally small for all three alloys.

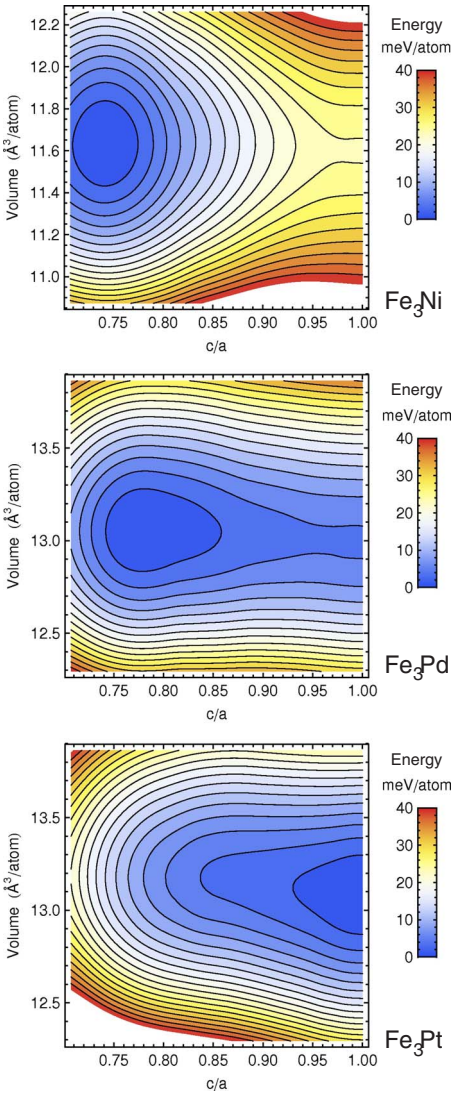

FIG. 3. (Color online) Contour plots of the binding surfaces (energy as a function of atomic volume v and tetragonal distortion c/a) of ferromagnetic $L1_2$ ordered Fe_3Ni (top), Fe_3Pd (center), and Fe_3Pt (bottom). The energy distance between two contour lines is 2 meV/atom. The global minima are located at $c/a=0.74$ and $v=11.633$ Å^3/atom for Fe_3Ni, $c/a=0.78$ and $v=13.054$ Å^3/atom for Fe_3Pd, and $c/a=1.00$ and $v=13.082$ Å^3/atom for Fe_3Pt.

It is with 22 meV/atom largest for Fe_3Ni and smallest for Fe_3Pd with only 4 meV/atom (minimum to saddle point). The shift of the minima agrees well with the fact that in the phase diagram of ordered Fe_3Pt the stability range of the body centered structures at $T=0$ K ends at higher Fe content compared to the other alloys as well as with the trend in the martensitic transition temperatures, which are reduced on variation in the second element from Ni to Pt. The maximum change in equilibrium volume associated with a full tetragonal transformation along the Bain path is small, less than one percent for all three alloys. There is also a strong experimental indication for an unusually flat energy surface. Recently, it has been shown that thin disordered $Fe_{70}Pd_{30}$ films can be grown epitaxially on different substrates inducing different lattice constants a in the film plane.[83] The corresponding perpendicular lattice constant, c, however, is free to adjust,

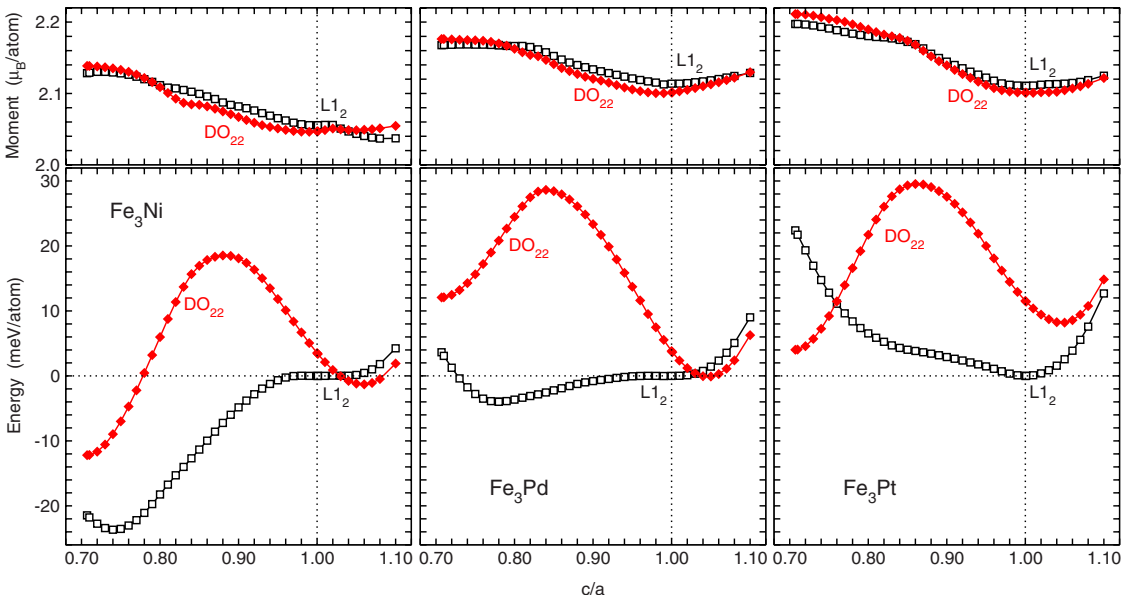

FIG. 4. (Color online) Comparison of total energy and magnetic moment as a function of tetragonal distortion c/a between $L1_2$-ordered and $D0_{22}$-ordered ferromagnetic Fe_3Ni (left), Fe_3Pd (center) and Fe_3Pt (right). The calculations were performed at a constant atomic volume close to the respective equilibrium volume of the $L1_2$ structure.

thereby realizing c/a ratios covering most of the Bain path. Such a strained epitaxial growth can only be expected if the energy associated with the lattice strain is sufficiently small along the Bain path.

The magnetic moment is largest on the bcc side, however, there is only little variation in the spin moments along the Bain path, which is of the order of 0.1 μ_B/atom (cf., Fig. 4). The slight variation in the magnitude between the alloys might well be attributed to the different equilibrium lattice constants.

B. $L1_2$ versus $D0_{22}$ order

For fcc alloys of stoichiometry A_3B, the $D0_{22}$ structure may be considered as another, possibly competing, realization of order. As can be seen from Fig. 1(d), the $D0_{22}$ structure emerges from the $L1_2$ structure by shifting one of the mixed planes half way along the diagonal without shearing the other planes. At the c/a ratio of the bcc lattice, the $D0_{22}$ structure turns into the highly symmetric $D0_3$ structure, which is equivalent to the Heusler-type $L2_1$ structure for a binary composition. For Fe_3Ni and Fe_3Pd, where order is not substantiated in experiment, the $D0_{22}$ becomes favored at c/a ratios slightly above one, as demonstrated in the lower panels of Fig. 4. For Fe_3Pt the $D0_{22}$ structure becomes favored at the bcc end. Only for this alloy, the energy of $D0_{22}$ becomes competitive with $L2_1$, taking into account the complete Bain path. The formation of a $D0_3$ phase in ordered near-stoichiometric Fe_3Pt might further be hindered by the slow kinetics of the necessary diffusive transformation at comparatively low temperatures. However, at the fcc side, the small energetic distance between $L1_2$ and $D0_{22}$ order indicates a low penalty and thus a comparatively high probability for antiphase boundaries in the ordered phases.

The magnetic response of both order types to a tetragonal distortion is identical. An important difference between $D0_{22}$ and $L2_1$ order is, however, that along the Bain path a considerable energy barrier exists for $D0_{22}$ but not for $L2_1$, which would slow down the transformation kinetics, if $D0_{22}$ could be stabilized.

IV. LATTICE DYNAMICS AND SOFT PHONONS

Important information about the stability of structures and potential relaxation mechanisms can be obtained from the phonon dispersion relations. Accordingly, extensive discussions have been taking place concerning martensitic precursor effects in the lattice dynamics of the austenitic phase in martensitically transforming alloys, which might yield, e.g., additional information on the transformation mechanisms. For the systems under consideration, experimentally determined phonon dispersion relations obtained by inelastic neutron scattering are available for disordered $Fe_{70}Ni_{30}$ and $Fe_{65}Ni_{35}$,[29,84] disordered $Fe_{72}Pd_{28}$,[22] and disordered as well as ordered Fe_3Pt.[21,23–28] Theoretical calculations of the full phonon dispersion, on the other hand, have been reported so far mainly for ordered Fe_3Ni,[65,81] disordered $Fe_{72}Pd_{28}$,[85,86] and Fe-Pd alloys in the Pd-rich composition range.[87–89] Several of the above mentioned investigations rely on empirical or semiempirical descriptions of the interatomic forces. Astonishingly, similar calculations for the Fe-Pt case appear to be missing. The inability of the experiment to provide a complete comparison of the ordered phases (which are easier to understand) together with the incomplete record of theoretical studies motivates our attempt to provide a comparative overview of the phonon dispersion of all three ordered isoelectronic alloys from first principles.

A. Phonon dispersion relations

The central feature of the phonon dispersions is the complete softening of the transversal acoustic branch TA_1 around

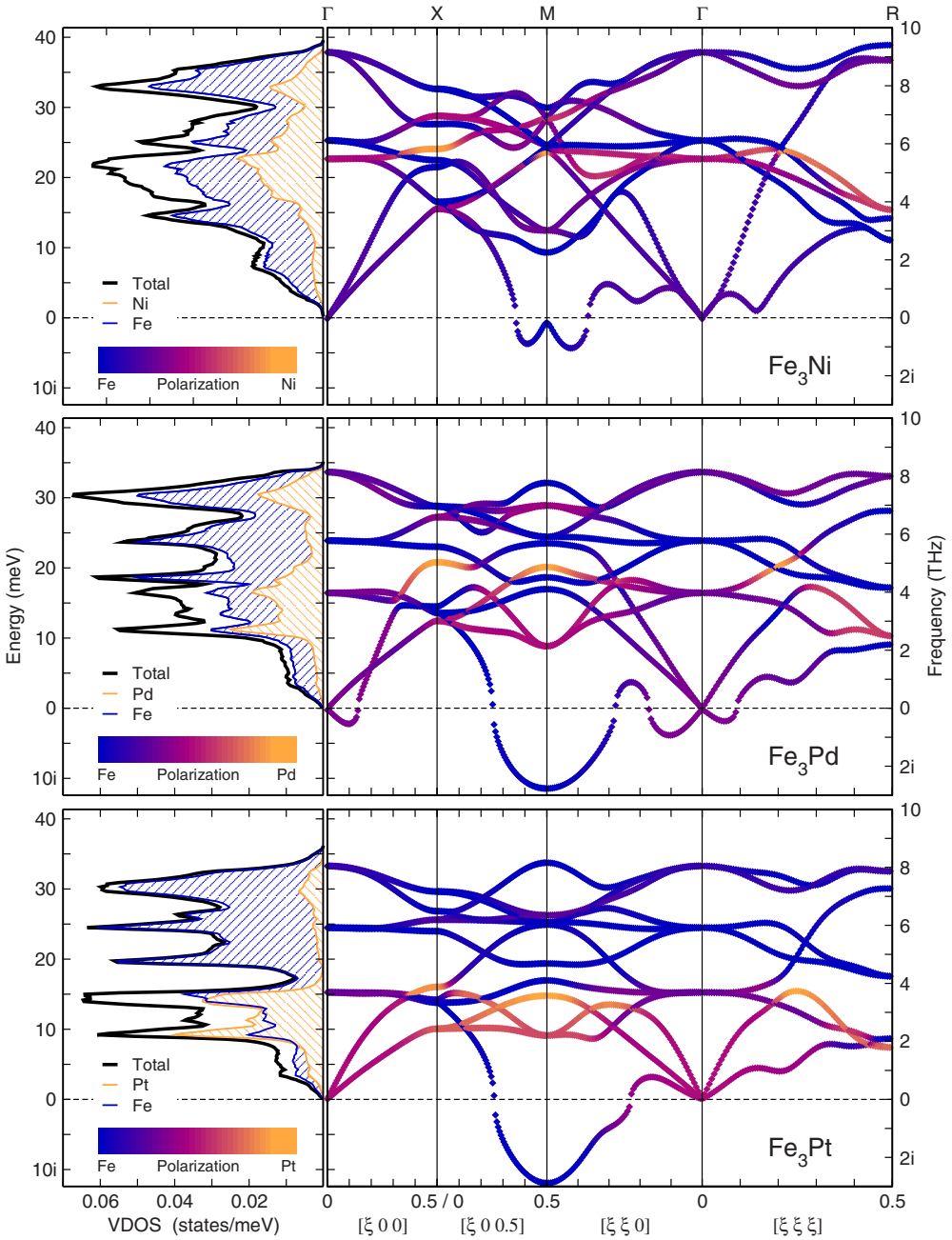

FIG. 5. (Color online) Calculated phonon dispersions (right panels) of $L1_2$ ordered Fe_3Ni (top), Fe_3Pd (center) and Fe_3Pt (bottom) along the main symmetry directions and the corresponding vibrational density of states (left panels). Imaginary frequencies are omitted from the density of states. The polarization of the phonon branches according to the atomic contributions to the respective eigenvectors is shown in the intensity (color) coding.

the *M* point. This is common for all three alloys, but most pronounced in Fe_3Pt. The occurrence of imaginary frequencies reflects the instability of the lattice which may gain energy by static atomic displacements according to the corresponding phonon mode. A strong anomalous softening of the TA_1 branch is a widely discussed observation from neutron diffraction experiments on ordered Fe_3Pt.[21,24,27,28] With decreasing temperature starting from the paramagnetic phase, the TA_1 mode becomes increasingly softer at the *M* point, finally reaching phonon energies as low as 3 meV for $T = 12$ K. The microscopic nature of the corresponding displacements will be discussed in the following section. An incomplete softening of the TA_1 branch with anomalous temperature dependence is also found for the disordered alloys. However, in these cases, it is far less pronounced and the wave vector is shifted toward the Γ-point.[22,27,29]

For Fe_3Pd one of the transversal acoustic modes in Fig. 5 starts with a negative slope from the Γ point, which indicates that the system might immediately undergo a long-wavelength distortion without activation barrier. This is not the case for Fe_3Ni, although here, the underlying structure is not the ground state, either. In both cases, the cubic $L1_2$ state describes only a saddle point. Thus the initial slope of the acoustic branches in the low energy and low wave vector

regime depends on small details of the binding surfaces and might well be affected by the specific choice of the method and technical setup, as demonstrated in Fig. 2. The softening along the [111] direction is strongest for Fe_3Ni. Both TA branches are degenerate, reaching frequencies as low as 1 meV around $\xi=0.14$. The corresponding eigenvectors are close to $(1,-1,0)$ and $(1,1,-2)$ and practically uniform for all four atoms in the primitive cells. This may correspond to the primary $[11\bar{2}]$ shear on (111) planes, common for martensitic transformation mechanisms of Fe-based alloys (e.g., see Refs. 5, 90, and 91).

The phonon dispersion of Fe_3Ni as shown in the upper panel of Fig. 5 agrees well with previous *ab initio* results for the same material obtained by the same method (but less restrictive accuracy).[65] Differences are mainly present at the *M* point, where the complete softening of the TA_1 mode is less pronounced in the present study and slightly shifted away from the Brillouin zone boundary. In addition, the softening in [111] direction is more pronounced in our study. Previous semiempirical calculations based on a tight-binding scheme on the other hand did only show comparable softening if the strength of the electron-phonon coupling was artificially enhanced.[81] This underlines the necessity to fully take into account the coupling between electronic and lattice degrees of freedom within a first-principles approach. Still, the convergence with respect to the subdivision in reciprocal space for the electronic structure as well as for the lattice dynamics remains an important issue.

Another quantity which allows for a detailed comparison with experiment is the element resolved vibrational density of states (VDOS) which is shown in the diagrams on the left of the dispersions. For alloys with a large mass difference, we expect a clear separation between the elemental contributions. This is indeed the case for Fe_3Pt, where we find a pseudogap at phonon energies around 17 meV. Above this energy, there is only little contribution from Pt vibrations, while we find a hybridization of Pt and Fe contributions in the energy range below. In Fe_3Pd, the Pd states move to higher energies, filling up the pseudogap and there is increased hybridization of the partial contributions at the optical bands in the uppermost part. This trend consequently continues for Fe_3Ni, moving the central peak of the partial VDOS of Ni up to an energy of 22.5 meV. In turn, the distinct low energy peak appearing around 10 meV for Fe_3Pt and Fe_3Pd has disappeared. In all three cases, there exists a significant contribution of Fe states in the low energy region (≤ 8 meV). The main peaks of the calculated VDOS agree well with experimental measurements of disordered $Fe_{65}Ni_{35}$ of Delaire and coworkers[92] as well as on ordered Fe_3Pt by Wiele *et al.*[93,94] and even recent measurements of the Fe-partial contributions of ordered Fe_3Pt nanoparticles by Roldan-Cuenya *et al.*[95] using the Mößbauer approach. The pseudogap, however, is not showing up in experimental VDOS as these generally experience a stronger broadening, which may be attributed to finite temperature of the measurements, resolution of the measurement devices and—not at last—the incomplete ordering usually present in Fe_3Pt samples.

The disappearance of the sharp energy peak in the VDOS around 10 meV points out a qualitative difference between Fe_3Ni and the other two alloys. In the latter case, these states are connected with vibrational modes at the *M* and the *R* points which are dominated by motions of the Pt or, respectively, Pd atoms as can be seen from the atomic polarization of the phonon dispersions shown in the intensity (color) coding in Fig. 5. In Fe_3Ni, however, the low lying modes in the vicinity of the *M* point mainly involve Fe atoms, which makes the Fe subsystem particularly soft and susceptible to element specific distortions, e.g., due to magnetoelastic coupling. In contrast, this feature completely disappears in the body centered cubic phase of Fe_3Ni, which we represent in our calculations for simplicity by the $D0_3$ ordered structure (cf. Fig. 6), as this also possesses cubic symmetry. Here, again, we find a rather clear separation between the Fe and the Ni contributions which now predominately occupy the low lying branches at the Brillouin zone boundary. In this sense, the situation bears similarity to the inversion of the Ni and Ga modes which was reported for the magnetic shape memory alloy Ni_2MnGa.[57,96,97]

B. Identification of the soft mode

As laid out in the previous paragraph, the two lowest frequencies in the dispersion of $L1_2$ Fe_3Ni at the *M* point involve only motions of the Fe species. Since the associated wave vector corresponds to the Brillouin zone boundary, the amplitudes are opposite at either end of the primitive cell. Therefore the term *antiferrodistortive transformation* has been has been coined for the condensation of the unstable phonon mode.[27] The displacements can be inferred from the corresponding eigenvectors and are sketched in Fig. 7. They belong to motions of the Fe-atoms either in direction of one of the two nearest neighbor Ni pairs, or perpendicular to this direction. If one describes the primitive cell as an Fe octahedron encaged by Ni atoms at the corner positions of the cube, the mode can be described in the first case as a rotational motion of the perimeter atoms in the (001) Fe plane, while the top and bottom atoms in the mixed plane remain in place. This kind of rotational mode is well known from perovskite structures, where oxygen octahedra form such tilted structures.[98,99] In the second case, it is rather described as a kind of breathing motion of the perimeter atoms in the Fe plane, where one half of the atoms move inwards and the other half move outward leading to an orthorhombic distortion of the Fe-octahedron. Keeping the terminology of Noda and Endoh as well as Kästner and co-workers, we will call these modes M4 and M2, respectively. Displacements according to both phonon modes lower the symmetry of the crystal and reduce the space group of the cubic $L1_2$ phase, $Pm\bar{3}m$ (number 221), to $P4/mbm$ (number 127). Since the latter is already tetragonal, a variation in c/a does not imply another change of symmetry, which corresponds well to the experimental reports of a low temperature fct phase.

As mentioned above, the nature of the distortions leading to the softening of the phonon modes can be inferred in principle from the eigenvectors of the dynamical matrix which can be constructed, e.g., by a Born-von-Karmann fit to the experimental dispersions. This indirect procedure often leaves room for ambiguities and has lead to a controversy

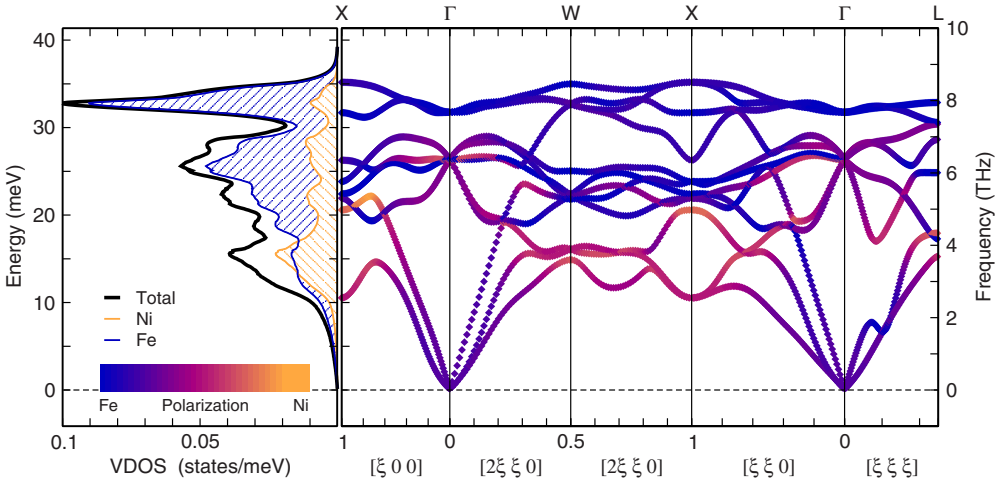

FIG. 6. (Color online) Calculated phonon dispersions (right panel) of $D0_3$ ordered Fe_3Ni along the main symmetry directions and the corresponding vibrational density of states (left panel). Again, the polarization of the phonon branches according to the atomic contributions to the respective eigenvectors is shown in the intensity (color) coding.

about the nature of the unstable mode in the past.[24,27] A more direct approach is to monitor the variation in the total energy as a function of the displacement according to the (frozen) phonon modes. This can be realized in a straight forward manner within a density functional theory approach. We construct $2\times2\times1$ supercells by doubling the primitive $L1_2$ cell in the plane of the atomic motion and apply the corresponding displacements δ as sketched in Fig. 7. The result, shown in Fig. 8, unambiguously proves that for all three alloys the M2 mode leads to a lower energy even for very small δ, explaining the imaginary frequencies at the M point. In Fe_3Pt and Fe_3Pd, the energy gain can reach values of about 5 meV/atom for displacements of about 0.08 to 0.09 Å. In Fe_3Ni this energy gain is significantly smaller and the minimum energy is obtained for smaller displacements. On the other hand, the M4 mode is considerably softer in Fe_3Ni than in the other two alloys. Here, the two lowest frequencies correspond to the two pure Fe modes, while for the other two alloys the second eigenvalue has a marked contribution of the heavier element. In the latter case, the M4 mode is represented by the fifth and the sixth eigenvalue with frequencies of 18.7 and 19.4 meV for Fe_3Pd and Fe_3Pt, respectively, as opposed to 9.3 meV for Fe_3Ni.

In this respect, it may be important to notice that a translation of the mixed (001) plane in $[1\bar{1}0]$ direction, which leads to an exchange of the Fe and Ni group atoms, transforms both modes, M2 and M4, in each other. Applying this transformation once every second unit cell transforms the

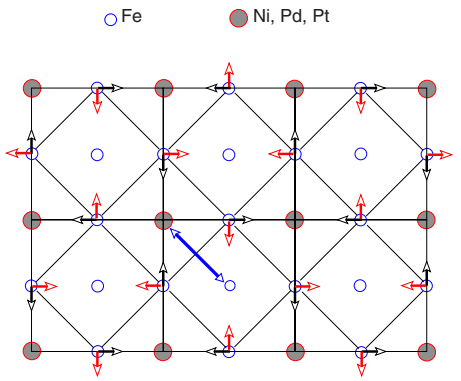

FIG. 7. (Color online) Schematic representation of the two M point soft modes in the phonon dispersions of fcc Fe_3Ni, Fe_3Pd, and Fe_3Pt shown in Fig. 5. The picture shows a projection of the repeated $L1_2$ unit cell along the [0 0 1] direction. The brighter (red) arrows correspond to the M2 mode, while the black arrows show vibrations of the M4 mode. The main feature here is that both vibrations are identical, but orthogonal to each other. Both vibrations match with a translation along one half of the face diagonal ([110] direction) as shown by the thick (blue) arrow, whereby the two vibrations remain the same but shifted in phase by π.

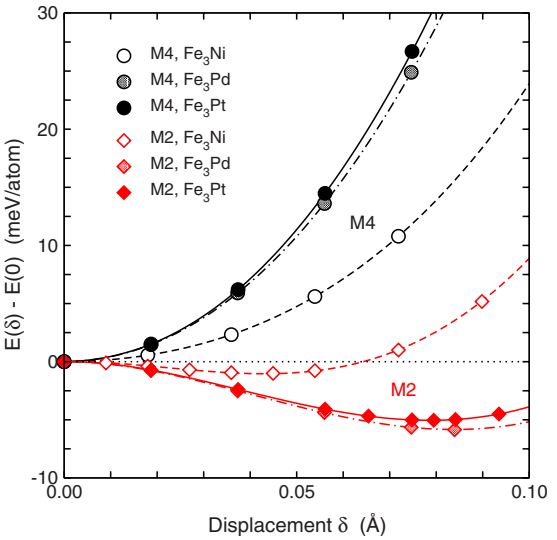

FIG. 8. (Color online) Total energy as a function of the displacement amplitude according to the two modes (M2, diamonds, and M4, circles) which may be made responsible for the (complete) softening of the acoustical phonons at the M point (cf. Fig. 7). Results are shown for Fe_3Ni, Fe_3Pd, and Fe_3Pt. The lines are polynomials fitted to the calculated data points. For all three alloys, displacements according to the M2 mode lead to a decrease in energy.

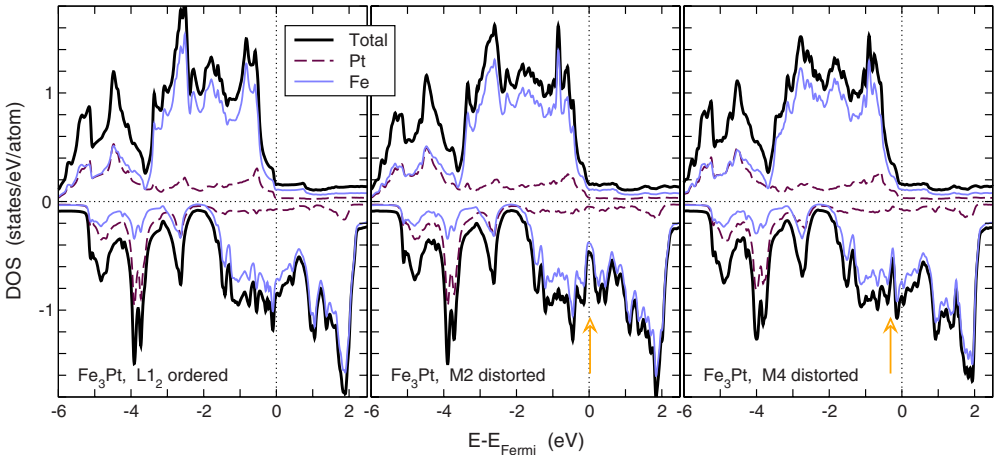

FIG. 9. (Color online) Comparison of the total and partial, site resolved electronic density of states (DOS) of Fe_3Pt with perfect $L1_2$ order (left) and M2 distorted Fe_3Pt with an displacement amplitude δ=0.0795 Å (center) and M4 distorted Fe_3Pt with δ=0.0748 Å (right). The majority spin DOS are denoted by positive values, while negative values refer to the minority spin channel. In the M2 case, a pseudogap opens at the Fermi level due to a redistribution of the Fe states. For the M4 distortion, a narrower gap opens up 0.25 eV below the Fermi level, while the DOS at the Fermi level remains largely unchanged (pseudogaps denoted by arrows).

$L1_2$ in $D0_{22}$ order, as can be seen from Fig. 1. $D0_{22}$ can thus also be regarded as an $L1_2$ structure with maximum density of antiphase boundaries. Thus atoms in the Fe plane will feel a superposition between both environments and displacements according to M2 and M4 modes become equivalent. Therefore, we expect that such distortions of the order will likely harden the soft phonon at the *M* point, especially for Fe_3Pd and Fe_3Pt.

C. Electronic origin of the antiferrodistortive transformation

While the total energy calculations supply us with the information that the imaginary phonon mode is related to an orthorhombic distortion of the Fe octahedra in the $L1_2$ unit cell, we are still left with the task to find the origin of this instability. A clue can be obtained from the comparison of the respective electronic density of states, which is shown paradigmatically in Fig. 9 for the undistorted, perfect $L1_2$ structure of Fe_3Pt as well as for supercells with M2 and M4 distortions. For all three cases, the majority spin density of states remains similar. The $L1_2$ DOS is in excellent agreement with the previous extensive study of Podgòrny,[73] apart from a small shift of the Fermi level in both spin channels which can be attributed to the use of an exchange-correlation functional without gradient corrections in Ref. 73. Fe_3Pt is at the onset of strong ferromagnetism, thus the *d* states of the majority spin channel are filled and the respective DOS is small at the Fermi energy, E_F, leaving no room for changes that could account for the structural distortions. This, however, does not apply for the minority spin channel, where a considerable number of *d* states is encountered right at E_F, especially for the undistorted $L1_2$ structure. The vast majority of these states comes from the Fe atoms, while the Pt DOS remains small, due to the nearly filled *d* shell and only moderate induced magnetic polarization of 0.36 μ_B.

On the other hand, the condensation of the M2 mode opens a deep pseudogap right at the Fermi level which is the indication of an extensive redistribution of states. In the spirit of a band-Jahn-Teller mechanism, lifting the degeneracy of electronic states at the Fermi level can lead to a net gain in band energy. This has been previously proposed as the main electronic mechanism leading to the tetragonal distortion in disordered magnetic shape memory Fe-Pd alloys.[75]

Accordingly, a distortion corresponding to the M4 mode does not decrease the number of states at E_F. Nevertheless, it opens another pseudogap 0.25 eV below the Fermi level. Although this gap is very narrow and should be expected to vanish already at rather low temperatures, it appears possible that a moderate decrease in the valence electron concentration e/a may bring this pseudogap to the Fermi level and possibly causes a change in the order of the modes at the *M* point which alters the corresponding ground-state structure.

The appearance of a pseudogap at E_F implies a severe reconstruction of the Fermi surface. Such reconstructions in connection with anomalous softening of the acoustic modes are a sign of strong electron-phonon coupling and frequently related to a Kohn anomaly. This involves a significant number of nesting states at E_F that can be connected with the same reciprocal vector which describes the anomaly in the phonon dispersions. Fermi-surface nesting and strong electron-phonon coupling in combination with transitions to modulated phases are commonly found in conventional and magnetic shape memory systems, as Ni-Al, Ni-Ti, and Ni-Mn-Ga.[30,100,101] In fact, the phonon softening in disordered Fe-Ni Invar has been related previously to a Kohn anomaly in the nonmagnetic state on the basis of first-principles calculations of ordered Fe_3Ni.[80] Here, we consider spin-polarized minority spin Fermi surfaces, i.e., the isosurfaces formed by the Kohn-Sham eigenvalues at the Fermi level in reciprocal space. These are depicted for Fe_3Ni and Fe_3Pt in Fig. 10 and we find good agreement of the shape with previous results obtained using WIEN2K.[102]

Six bands are crossing E_F in the minority spin channel making the Fermi surfaces quite complex objects. Nevertheless, it is possible to relate nesting behavior to two of these bands, the 13th and the 15th band which are shown sepa-

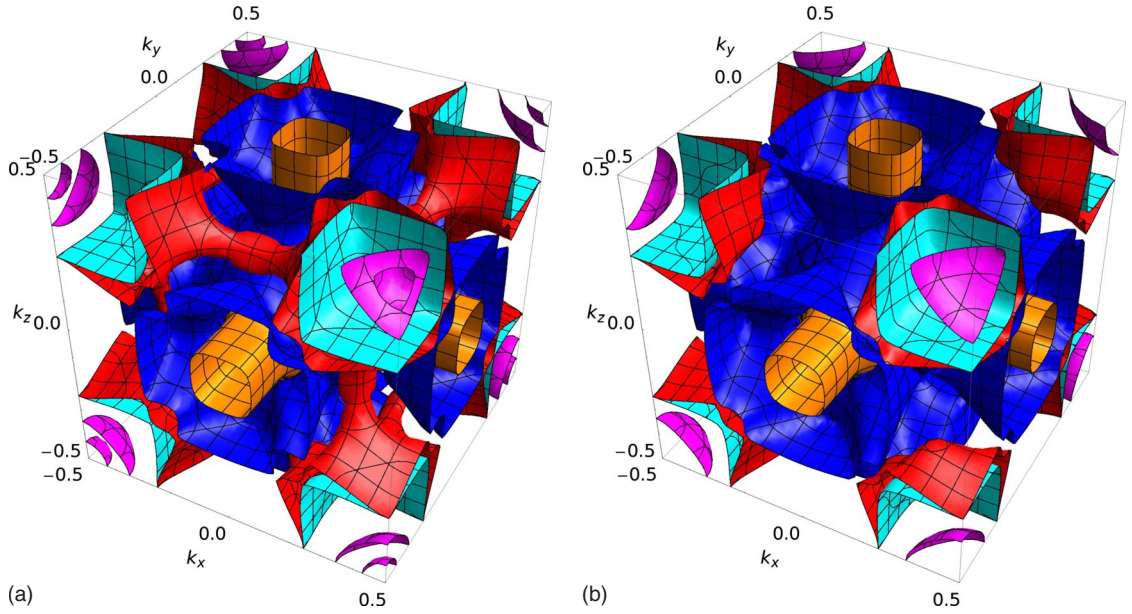

FIG. 10. (Color online) Plots of the isoenergy surface in reciprocal space of the minority spin electronic states the Fermi level (Fermi surface) of Fe_3Ni (left) and Fe_3Pt (right). The Fermi level is intersected by six bands (shown online in different colors). The features are largely similar and differ mainly only in size due to the varying atomic volumes. Both surfaces exhibit large nearly flat portions which may give rise to a Kohn anomaly.

rately in Fig. 11. The 13th minority spin band represents an extended spherical hole pocket around the Γ-point with hopper-shaped extrusions reaching the Brillouin zone boundary. Facilitated by the cubic symmetry, the flattened, horizontal walls of these extrusions can provide nesting with a vector of exactly $(\frac{1}{2},\frac{1}{2},0)$, c.f., Fig. 11(a). These parts are connected by a tangential nesting vector, which is insensitive to a specific value of q and not expected to produce a sharp contribution to the generalized susceptibility. There is another possibility for nesting between the Fermi surfaces of 13th and the 15th band. The 15th band forms a cubic electron pocket around the R point as depicted in Fig. 11(b). The walls of the cubes are nearly located on the same plane as the flattened parts of the 13th band. This plane is parallel to the boundary of the cubic Brillouin zone. Two of them exist in each of the cubic directions, such that nesting can occur be-

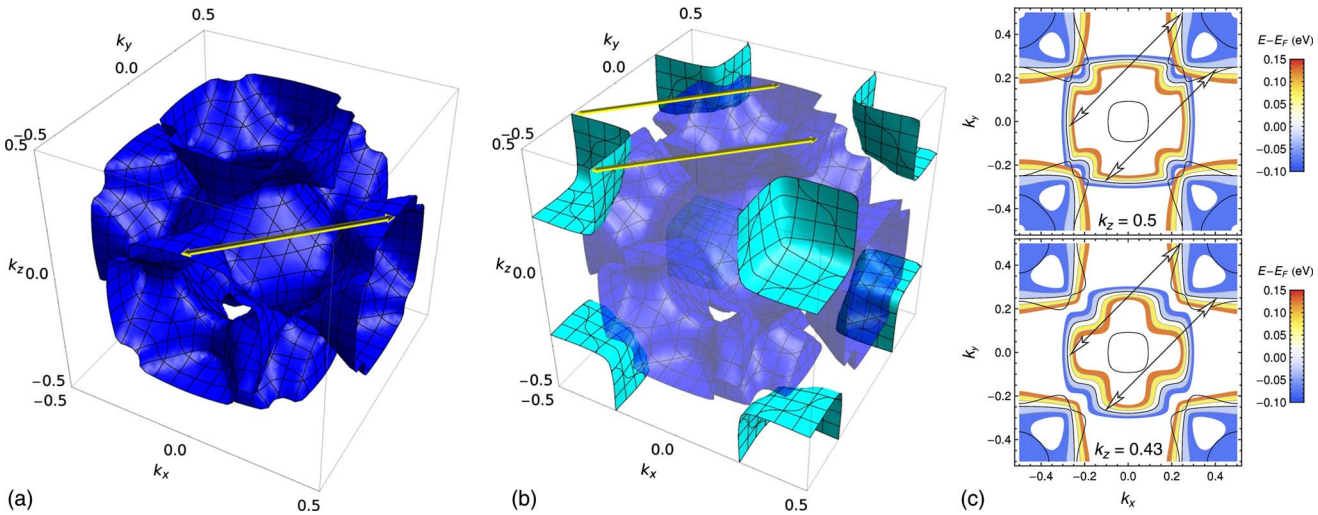

FIG. 11. (Color online) Fermi surfaces of the 13th (a) and 15th (b) minority spin band of Fe_3Pt (with an additional semitransparent image of the 13th band in the latter case). These two bands exhibit flat parts which may be connected with a wave vector close to $(\frac{1}{2},\frac{1}{2},0)$ as indicated by the arrows. The vector can either be applied tangentially between the flattened, horizontal walls of the cone-shaped extensions at the zone boundary entirely within the surface of the 13th band as shown in (a) or between the vertical walls on the left and the respective sections of the cube shaped surface centered around the R point in (b). The eigenvalues in reciprocal space of the of the 13th and 15th bands along two horizontal planes (k_z=0.5 and k_z=0.43) are shown in (c) as contour plots. The intersection of the complete Fermi surface (all bands) with these planes are marked by black lines. The arrows denote again parallel vectors $(\frac{1}{2},\frac{1}{2},0)$. The energies are given relative to the Fermi level; the difference between two contour lines is 50 meV.

tween the two bands on the two different planes, respectively. The correspondence in this case is not necessarily exactly $(\frac{1}{2},\frac{1}{2},0)$ and in direction of the face diagonal, but it can be expected to provide a pronounced peak in the generalized susceptibility and thus a considerable contribution to electron-phonon coupling. The cross sections in Fig. 11(c), taken at two different values of k_z, demonstrate that this correspondence is not restricted to the zone boundary, but rather affects a significant portion of the Fermi surface. For Fe_3Ni the hopper-shaped extrusions of the 13th band are smaller and the cubes larger than in the Fermi-surface of Fe_3Pt, which results in a smaller distance between the parallel planes and thus a smaller length of the q vector. This coincides nicely with the shift of the instability in the TA_1 branch away from the M, point as well as the smaller magnitude of the imaginary eigenvalue.

It should be mentioned that a thorough investigation of the relation between Fermi surface nesting and transformative processes requires a detailed statistics, e.g., an evaluation of the generalized susceptibility with respect to all contributing reciprocal vectors as well as the calculation of the electron-phonon coupling matrix elements. This is a formidable task in itself and beyond the scope of this work. Nevertheless, in our view, the purely graphical discussion above gives already sufficient arguments that a Kohn anomaly is responsible for the low temperature structural changes in the ordered alloys.

V. CONCLUSIONS

Within the present investigation, we systematically compared structural, electronic and dynamic properties of ordered Fe-rich alloys with the elements of the Ni-group. The only one of these three alloy, which can be obtained experimentally in the ordered state, Fe_3Pt, is also the only one which possesses an fcc ground-state structure. The dominant type of ordering in all three alloys is $L1_2$, in accordance with experimental observation. Competing $D0_{22}$ order was observed for hypothetical Fe_3Ni and Fe_3Pd for fct structures with a tetragonal distortion $c/a>1$ and for Fe_3Pt with bcc coordination. However, for ideal fcc $(c/a=1)$, $D0_{22}$ order is well within the range of thermal energies, suggesting that antiphase boundaries are very likely to appear in the cubic $L1_2$ phases.

The phonon dispersions of the three alloys possess as a common feature a complete softening of TA_1 branch in [110] direction around the M point, which is strongest for Fe_3Pt and Fe_3Pd as well as a partial softening along the [111] direction. The first leads to the freezing of the respective phonon mode (M2) which can be identified as an orthorhombic distortion of the Fe octahedra in the primitive $L1_2$ cell without involving the Ni-group elements. The second anomaly becomes increasingly pronounced with decreasing mass of the Ni-group element, as this leads effectively to an increased Fe contribution to the low energy acoustical phonons.

It may be speculated whether the rather smeared out softening of the TA_1 branch in [110] direction in the disordered alloys can be interpreted in terms of a corresponding distortion with similar electronic origin, but on a larger, statistically modified period. This owes to the fact that the Fe octahedra can be considered to be statistically distributed within the bulk alloy and result finally in a rather broadened and less pronounced anomaly. These octahedra are characteristic for the $L1_2$ structure, but also other locally Fe-enriched cluster configurations, which are more or less susceptible to deformations, may contribute. Similarly, the gross electronic structure will appear rather smeared out for the disordered crystal, but distinct features may prevail locally within suitable Fe-clusters and induce corresponding local distortions. Indeed, characteristic relaxations of the atomic positions have been reported in *ab initio* calculations for fcc FeNi-Invar alloys for 64-atom quasirandom structures.[103] This also fits well with our observation that in Fe_3Ni not only the M2 mode but also the orthogonal M4 mode becomes rather soft at the M point, which makes collective motions in the Fe-(001) planes very cost effective. Furthermore, own investigations considering structural relaxations of 108-atom Fe-Pd and Fe-Pt supercells with random distribution of atoms, yield a considerable energy gain from a similar relaxation process.[104]

The sum of these observations supports the view that the origin of the anomalous features in the acoustical branches can be attributed solely to the Fe species. This is confirmed by the calculation of the electronic structure of the $L1_2$ ordered and the distorted alloys. The condensation of the M2 mode opens a pseudogap in the minority density of states right at the Fermi level, reducing the density of states by nearly 50%. Again, only contributions from Fe states are involved. The origin for this strong reconstruction of the Fermi surface can be related to extended flat areas which nest with a reciprocal vector of nearly $(\frac{1}{2},\frac{1}{2},0)$ which corresponds to the softening of the TA_1 phonon mode at the M point.

The subtle interdependence between electronic structure at the Fermi level and the antiferrodistortive transformation confirms once more that the valence electron density, which controls the overall filling of the minority spin channel on a fine level, is one of the key factors for the design of Fe-rich functional alloys. On the basis of our investigation, we further conclude—in accordance with Ref. 75—that the specific concentration of the Fe species must be considered as another important quantity and, additionally, the mass of the alloying elements which modifies the lattice dynamics related to the low lying acoustical modes.

ACKNOWLEDGMENTS

The authors gratefully acknowledge helpful remarks and discussions with S. Fähler (Dresden), W. Keune (Duisburg-Essen), J. Neuhaus (München), B. Sanyal (Uppsala) and E. F. Wassermann (Duisburg-Essen). Part of the calculations was carried out on the JUGENE supercomputer of the John von Neumann Institute for Computing, Forschungszentrum Jülich. We thank the staff of Jülich Supercomputing Center for their continuous support. Financial support was granted by the Deutsche Forschungsgemeinschaft in the frame of the priority program SPP 1239, *Change of microstructure and shape of solid materials by external magnetic fields*.

*markus.gruner@uni-due.de

[1] C.-E. Guillaume, C. R. Hebd. Seances Acad. Sci. **125**, 235 (1897).
[2] E. F. Wassermann, in *Ferromagnetic Materials*, edited by K. H. J. Buschow and E. P. Wohlfahrt (Elsevier, Amsterdam, 1990), Vol. 5, Chap. 3, p. 237.
[3] M. Shiga, in *Materials Science and Technology*, edited by R. W. Cahn, P. Haasen, and E. J. Kramer (VCH, Weinheim, 1994), Vol. 3B, Chap. 10, p. 159.
[4] E. F. Wassermann and M. Acet, in *Magnetism and Structure in Functional Materials*, Springer Series in Materials Science Vol. 79, edited by A. Planes, L. Manõsa, and A. Saxena (Springer, Berlin, 2005), p. 177.
[5] Z. Nishiyama, *Martensitic Transformation* (Academic Press, New York, 1978).
[6] W. Pepperhoff and M. Acet, *Constitution and Magnetism of Iron and its Alloys*, Engineering Materials Vol. III (Springer, Berlin, Heidelberg, New York, 2001).
[7] R. D. James and M. Wuttig, Philos. Mag. A **77**, 1273 (1998).
[8] R. Hayashi, S. Murray, M. Marioni, S. Allen, and R. OHandley, Sens. Actuators **81**, 219 (2000).
[9] T. Kakeshita and T. Fukuda, Mater. Sci. Forum **394-395**, 531 (2002).
[10] T. Fukuda, T. Sakamoto, T. Kakeshita, T. Takeuchi, and K. Kishio, Mater. Trans. **45**, 188 (2004).
[11] T. Kakeshita, T. Fukuda, and T. Takeuchi, Mater. Sci. Eng., A **438-440**, 12 (2006).
[12] K. Ullakko, J. K. Huang, C. Kantner, R. C. O'Handley, and V. V. Kokorin, Appl. Phys. Lett. **69**, 1966 (1996).
[13] A. Sozinov, A. A. Likhachev, N. Lanska, and K. Ullakko, Appl. Phys. Lett. **80**, 1746 (2002).
[14] O. Söderberg, Y. Ge, A. Szinov, S.-P. Hannula, and V. V. Lindroos, Smart Mater. Struct. **14**, S223 (2005).
[15] V. A. Chernenko, C. Segui, E. Cesari, J. Pons, and V. V. Kokorin, Phys. Rev. B **57**, 2659 (1998).
[16] V. V. Khovaylo, V. D. Buchelnikov, R. Kainuma, V. V. Koledov, M. Ohtsuka, V. G. Shavrov, T. Takagi, S. V. Taskaev, and A. N. Vasiliev, Phys. Rev. B **72**, 224408 (2005).
[17] M. Richard, J. Feuchtwanger, D. Schlagel, T. Lograsso, S. Allen, and R. O'Handley, Scr. Mater. **54**, 1797 (2006).
[18] M. Matsui, H. Yamada, and K. Adachi, J. Phys. Soc. Jpn. **48**, 2161 (1980).
[19] S. Muto, R. Oshima, and F. E. Fujita, Metall. Trans. A **19**, 2723 (1988).
[20] J. Cui, T. W. Shield, and R. D. James, Acta Mater. **52**, 35 (2004).
[21] K. Tajima, Y. Endoh, Y. Ishikawa, and W. G. Stirling, Phys. Rev. Lett. **37**, 519 (1976).
[22] M. Sato, B. H. Grier, S. M. Shapiro, and H. Miyajima, J. Phys. F: Met. Phys. **12**, 2117 (1982).
[23] Y. Noda, Y. Endoh, S. Katano, and M. Iizumi, Physica **120B**, 317 (1983).
[24] Y. Noda and Y. Endoh, J. Phys. Soc. Jpn. **57**, 4225 (1988).
[25] M. Schwoerer-Böhning, S. Klotz, J. M. Besson, E. Burkel, M. Braden, and L. Pintschovius, Physica B **219-220**, 479 (1996).
[26] M. Schwoerer-Böhning, S. Klotz, J. M. Besson, E. Burkel, M. Braden, and L. Pintschovius, Europhys. Lett. **33**, 679 (1996).
[27] J. Kästner, W. Petry, S. Shapiro, A. Zheludev, J. Neuhaus, T. Roessel, E. Wassermann, and H. Bach, Eur. Phys. J. B **10**, 641 (1999).
[28] J. Kästner, J. Neuhaus, E. Wassermann, W. Petry, B. Hennion, and H. Bach, Eur. Phys. J. B **11**, 75 (1999).
[29] E. Maliszewski and S. Bednarski, Phys. Status Solidi B **211**, 621 (1999).
[30] Y. Lee, J. Y. Rhee, and B. N. Harmon, Phys. Rev. B **66**, 054424 (2002).
[31] C. Bungaro, K. M. Rabe, and A. Dal Corso, Phys. Rev. B **68**, 134104 (2003).
[32] A. T. Zayak, P. Entel, J. Enkovaara, A. Ayuela, and R. M. Nieminen, Phys. Rev. B **68**, 132402 (2003).
[33] T. Hickel, M. Uijttewaal, B. Grabowski, and J. Neugebauer, Mater. Res. Soc. Symp. Proc. E **1050**, BB03-02 (2008).
[34] M. E. Gruner and P. Entel, J. Phys.: Condens. Matter **21**, 293201 (2009).
[35] M. Uhl, L. M. Sandratskii, and J. Kübler, Phys. Rev. B **50**, 291 (1994).
[36] M. van Schilfgaarde, I. A. Abrikosov, and B. Johansson, Nature (London) **400**, 46 (1999).
[37] I. A. Abrikosov, A. E. Kissavos, F. Liot, B. Alling, S. I. Simak, O. Peil, and A. V. Ruban, Phys. Rev. B **76**, 014434 (2007).
[38] P. Hohenberg and W. Kohn, Phys. Rev. **136**, B864 (1964).
[39] G. Kresse and J. Furthmüller, Phys. Rev. B **54**, 11169 (1996).
[40] G. Kresse and D. Joubert, Phys. Rev. B **59**, 1758 (1999).
[41] P. E. Blöchl, Phys. Rev. B **50**, 17953 (1994).
[42] P. E. Blöchl, O. Jepsen, and O. K. Andersen, Phys. Rev. B **49**, 16223 (1994).
[43] J. P. Perdew, in *Electronic Structure of Solids '91*, edited by P. Ziesche and H. Eschrig (Akademie Verlag, Berlin, 1991).
[44] S. H. Vosko, L. Wilk, and M. Nusair, Can. J. Phys. **58**, 1200 (1980).
[45] J. P. Perdew, K. Burke, and M. Ernzerhof, Phys. Rev. Lett. **77**, 3865 (1996).
[46] J. P. Perdew, K. Burke, and Y. Wang, Phys. Rev. B **54**, 16533 (1996).
[47] It should be mentioned at this point, that for heavy elements, as the 5*d* transition metal Pt, a fully relativistic treatment would be superior in general. In the present case, this also implies to go beyond the frequently employed perturbative corrections, because fully self-consistently obtained charge densities are needed for the calculation of the interatomic forces, which are used to determine the respective phonon dispersion relations. Within the VASP code, spin-orbit terms are only available in connection with a noncollinear representation of magnetic moments, which significantly increases the computational demands while slowing down convergence. On the other hand, the benefit would be rather limited, because the essential physics is governed by a redistribution of Fe 3*d* states in the vicinity of the Fermi level, as laid out in the further course of the paper. For our purposes, we therefore restrict to the scalar relativistic approach, allowing us to treat all three alloys consistently on the same level of approximation at reasonable numerical cost.
[48] E. C. Bain, Trans. Am. Inst. Min., Metall. Pet. Eng. **70**, 25 (1924).
[49] P. Blaha, K. Schwarz, G. K. H. Madsen, D. Kvasnicka, and J. Luitz, *WIEN2k, An Augmented Plane Wave+Local Orbitals Program for Calculating Crystal Properties* (Karlheinz Schwarz, Techn. Universität Wien, Austria, 2001).
[50] N. Zotov and A. Ludwig, Intermetallics **16**, 113 (2008).
[51] X. Gonze and C. Lee, Phys. Rev. B **55**, 10355 (1997).
[52] K. Parlinski, Z-. Q. Li, and Y. Kawazoe, Phys. Rev. Lett. **78**,

4063 (1997).
[53] G. Kresse, J. Furthmüller, and J. Hafner, Europhys. Lett. **32**, 729 (1995).
[54] R. Resta, in *Festkörperplobleme: Advances in Solid-State Physics*, edited by P. Gross (Vieweg, Braunschweig, 1985), Vol. 25, p. 183.
[55] A. Dal Corso and S. de Gironcoli, Phys. Rev. B **62**, 273 (2000).
[56] K. Parlinski, Mater. Sci. (Poland) **23**, 357 (2005).
[57] A. T. Zayak, P. Entel, K. M. Rabe, W. A. Adeagbo, and M. Acet, Phys. Rev. B **72**, 054113 (2005).
[58] P. Entel, M. E. Gruner, W. A. Adeagbo, and A. Zayak, Mater. Sci. Eng., A **481-482**, 258 (2008).
[59] M. E. Gruner, W. A. Adeagbo, A. T. Zayak, A. Hucht, S. Buschmann, and P. Entel, Eur. Phys. J. Spec. Top. **158**, 193 (2008).
[60] D. Alfè, Comput. Phys. Commun. **180**, 2622 (2009).
[61] D. Alfè, program available at http://chianti.geol.ucl.ac.uk/~dario
[62] http://www.pwscf.org
[63] D. Vanderbilt, Phys. Rev. B **41**, 7892 (1990).
[64] Fe.pbe-nd-rrkjus.UPF, Ni.pbe-nd-rrkjus.UPF and Fe.pz-sp-van_ak.UPF, Pt.pz-rrkjus.UPF, available from: http://www.pwscf.org/pseudo/1.3/UPF
[65] W. A. Adeagbo, A. T. Zayak, and P. Entel, Phase Transit. **79**, 853 (2006).
[66] V. L. Moruzzi, Physica B **161**, 99 (1989).
[67] V. L. Moruzzi, Phys. Rev. B **41**, 6939 (1990).
[68] D. D. Johnson, F. J. Pinski, J. B. Staunton, B. L. Györffy, and G. M. Stocks, in *Physical Metallurgy of Controlled Expansion Invar-Type Alloys*, edited by K. C. Russel and D. F. Smith (The Minerals Metals & Materials Society, Warrendale, 1990), p. 3.
[69] P. Entel, E. Hoffmann, P. Mohn, K. Schwarz, and V. L. Moruzzi, Phys. Rev. B **47**, 8706 (1993).
[70] M. Schröter, H. Ebert, H. Akai, P. Entel, E. Hoffmann, and G. G. Reddy, Phys. Rev. B **52**, 188 (1995).
[71] S. Khmelevskyi, I. Turek, and P. Mohn, Phys. Rev. Lett. **91**, 037201 (2003).
[72] S. Khmelevskyi and P. Mohn, Phys. Rev. B **69**, 140404(R) (2004).
[73] M. Podgórny, Phys. Rev. B **43**, 11300 (1991).
[74] Zs. Major, S. B. Dugdale, T. Jarlborg, E. Bruno, B. Ginatempo, J. B. Staunton, and J. Poulter, J. Phys.: Condens. Matter **15**, 3619 (2003).
[75] I. Opahle, K. Koepernik, U. Nitzsche, and M. Richter, Appl. Phys. Lett. **94**, 072508 (2009).
[76] M. B. Taylor, B. L. Gyorffy, and C. J. Walden, J. Phys.: Condens. Matter **3**, 1575 (1991).
[77] Y. Chen, T. Atago, and T. Mohri, J. Phys.: Condens. Matter **14**, 1903 (2002).
[78] R. A. Stern, S. D. Willoughby, J. M. MacLaren, J. Cui, Q. Pan, and R. D. James, J. Appl. Phys. **93**, 8644 (2003).
[79] S. Lipiński and M. Pugaczowa-Michalska, Physica B **269**, 227 (1999).
[80] E. Hoffmann, H. Herper, P. Entel, S. G. Mishra, P. Mohn, and K. Schwarz, Phys. Rev. B **47**, 5589 (1993).
[81] H. Herper, E. Hoffmann, P. Entel, and W. Weber, J. Phys. IV **5**, C8-293 (1995).
[82] *Phase Diagrams of Binary Iron Alloys*, Monograph Series on Alloy Phase Diagrams Vol. 9, edited by H. Okamoto (ASM International, Materials Park, Ohio, USA, 1993).
[83] J. Buschbeck, I. Opahle, M. Richter, U. K. Rößler, P. Klaer, M. Kallmayer, H. J. Elmers, G. Jakob, L. Schultz, and S. Fähler, Phys. Rev. Lett. **103**, 216101 (2009).
[84] E. D. Hallman and B. N. Brockhouse, Can. J. Phys. **47**, 1117 (1969).
[85] I. Akgün and G. Ugur, Nuovo Cimento D **19**, 779 (1997).
[86] A. F. Xavier, R. J. B. Balaguru, S. A. C. Raj, and N. Lawrence, Indian J. Phys. **81**, 455 (2007).
[87] S. Ghosh, J. Phys.: Condens. Matter **20**, 275208 (2008).
[88] B. Dutta and S. Ghosh, J. Phys.: Condens. Matter **21**, 095411 (2009).
[89] S. Ghosh, Intermetallics **17**, 708 (2009).
[90] M. S. Wechsler, T. A. Read, and D. S. Lieberman, Trans. AIME **218**, 202 (1960).
[91] M. Ahlers, Philos. Mag. A **82**, 1093 (2002).
[92] O. Delaire, M. Kresch, and B. Fultz, Philos. Mag. **85**, 3567 (2005).
[93] N. Wiele, H. Franz, and W. Petry, Physica B **263-264**, 716 (1999).
[94] N. Wiele, Ph.D. thesis, Technische Universität München, 2001.
[95] B. Roldan Cuenya, J. R. Croy, L. K. Ono, A. Naitabdi, H. Heinrich, W. Keune, J. Zhao, W. Sturhahn, E. E. Alp, and M. Hu, Phys. Rev. B **80**, 125412 (2009).
[96] A. T. Zayak, W. A. Adeagbo, P. Entel, and K. M. Rabe, Appl. Phys. Lett. **88**, 111903 (2006).
[97] P. Entel, V. D. Buchelnikov, V. V. Khovailo, A. T. Zayak, W. A. Adeagbo, M. E. Gruner, H. C. Herper, and E. F. Wassermann, J. Phys. D **39**, 865 (2006).
[98] P. Ghosez, E. Cockayne, U. V. Waghmare, and K. M. Rabe, Phys. Rev. B **60**, 836 (1999).
[99] K. Parlinski and Y. Kawazoe, Eur. Phys. J. B **16**, 49 (2000).
[100] X. Huang, I. I. Naumov, and K. M. Rabe, Phys. Rev. B **70**, 064301 (2004).
[101] G. L. Zhao and B. N. Harmon, Phys. Rev. B **48**, 2031 (1993).
[102] S. Wakoh, M. Matsumoto, and I. Matsumoto, J. Phys. Soc. Jpn. **71**, 1393 (2002).
[103] F. Liot and I. A. Abrikosov, Phys. Rev. B **79**, 014202 (2009).
[104] M. E. Gruner, (unpublished).